Journal of Engineering Science and Technology
Vol. 10, No. 4 (2015) 509 - 525


# STUDIES ON ENERGY PENETRATION AND MARANGONI EFFECT DURING LASER MELTING PROCESS

K. ANTONY*, N. ARIVAZHAGAN

School of Mechanical and Building Sciences, VIT University, India 632014
School of Mechanical and Building Sciences,
VIT University, India 632014,
*Corresponding author: kurianantony@vit.ac.in

**Abstract**

Many additive manufacturing processes use energy from laser beam to melt powder particles to form layered objects. This paper mainly focused its attention on some of the major factors which plays a vital role during laser melting, namely energy penetration, shrinkage, absorptivity and Marangoni effect. A study was performed to simulate and validate the effect of energy density on Marangoni effect and energy penetration. Analytical solutions to moving heat source problems were developed and their effects on process parameters viz. energy penetration through a layer of powder particles were validated. The numerical investigations demonstrated the significant effect of energy density on laser beam towards the laser track. Finally, experiments were performed to validate the simulations using Nd: YAG laser on SS316L powder particles. Thus this study would enable in optimizing the process parameters of the additive manufacturing process.

Keywords: Selective laser melting, Energy density, Marangoni effect, Absorptivity.

## 1. Introduction

Many additive manufacturing processes allow complex objects to be built by selectively fusing together successive layers of powdered material Williams and Deckard [1]. In most of these processes, energy from laser beam is used to melt powder particles to form layers of complex shaped three-dimensional (3D) parts directly from metal powder [2, 3]. Compared to other additive manufacturing processes, properties comparable to those of bulk materials [4]. The laser melting process is laser based processes have the advantage to produce parts that have

**Nomenclatures**

| | |
|---|---|
| $D$ | Average diameter of powder particle, μm |
| $E\rho$ | Energy density, J/mm$^2$ |
| $L$ | Length of the free surface, m or Layer thickness, μm |
| $M_a$ | Dimensionless Marangoni number |
| $P$ | Laser power, W |
| $r$ | Beam radius, μm |
| $u$ | Velocity vector, m/s |
| $v$ | Scan speed, m/min |

***Greek Symbols***

| | |
|---|---|
| $\alpha$ | Absorptivity of the dense material |
| $\beta$ | Extinction coefficient |
| $\Delta\sigma$ | Surface tension difference |
| $\varepsilon$ | Porosity, % |
| $\eta$ | Dynamic viscosity, kg/m·s |
| $\lambda$ | Optical depth |
| $\rho$ | Density, kg/m$^3$ |
| $\upsilon$ | Kinematic viscosity, m$^2$/s |

mechanical rather complex and involves many different physical phenomena involving multiple modes of heat, mass, and momentum transfer [5]. In addition, the temperature field in the powder bed varies quickly with high laser scan speed, leading to the solid-liquid-solid phase transformation within a very short time period.

The rapid phase transformation is usually accompanied by a large interfacial force, thus balling effect or distortion might occur if the laser processing parameters are not properly selected [6]. The quality of each molten layer strongly depends on the condition of temperature distribution and energy density [7].

During laser melting process, the energy transformation, momentum transformation and mass transformation are influenced by the thermal phenomena because of the heat transfer from the energy of laser beam to the powder during melting. The phenomena are conduction, convection and radiation effects in the powder bed which have an impact on the quality of products which is highly dependent on the factor of transient melting temperature [8]. Bai et al. [9] presented a two dimensional finite element model to predict the temperature field during laser melting of polymer-coated molybdenum powder. Gusarov et al. [10] proposed a model for coupled radiation transfer and thermal diffusion, which allocates a local temperature field. The author also stated that the freshly deposited powder is not mechanically compressed in the SLM machine in order to damage the underlying consolidated part. Therefore, it has a high porosity as freely spread powder, which is in the range 40–60% for typical metallic powders.

The major processes variables which influence laser melting are laser power, scan speed, layer thickness scan spacing and spot size. Figures 1 and 2 give an outline on different physical phenomena as well as process parameters acting on the laser sintering / melting process. These process parameters together with material properties individually or collectively influence the various physical phenomena such as energy penetration, heat conduction, capillary forces, Melting/Solidification, radiation, wetting, Marangoni effect, distortion, curling,

balling [11]. Laser melting is characterized by a deep interaction between heat, mass and momentum transfer along with chemical transitions and variations of the mechanical and thermo-physical properties of the materials [12].

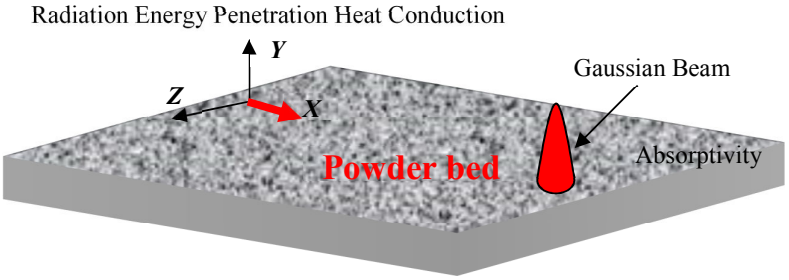


**Fig. 1. Process parameters and physical phenomena during laser sintering process.**

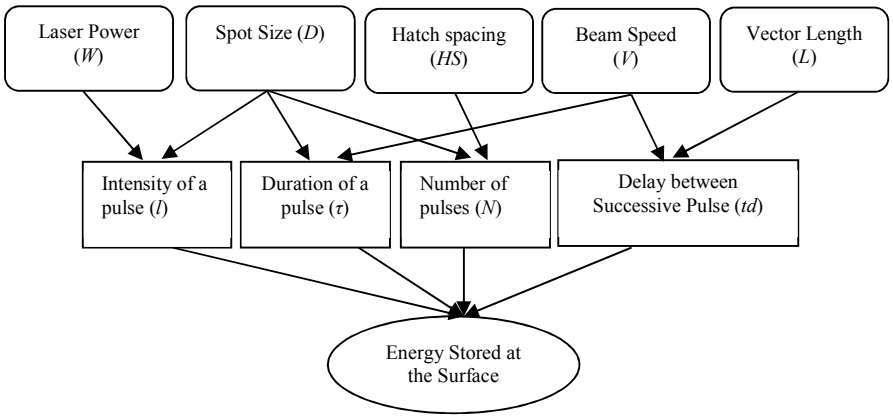


**Fig. 2. Influence of process parameters on the energy stored on the surface.**

Energy density of the laser beam is denoted by the equation [13]:

$$E\rho = \frac{P}{vd} \tag{1}$$

where $E\rho$ is the Energy Density (J/mm$^2$); $P$ is the laser power; $v$ is the scan speed or the velocity by which the laser beam moves over the powder surface, $d$ is the spot diameter.

In general, as the energy density input increases higher fractional density of powder is obtained. The density is linearly proportional to the ratio of laser power to scan speed. It is also reported that, with decreasing the line scan spacing higher density is obtained [7]. Fischer et al. [14] noted that the energy deposition is performed by both bulk-coupling and powder-coupling mechanisms when interaction of laser radiation with metal powders occurs. The density change during irradiation and formation of metal agglomerates also affect the coupling

efficiency and thus influence the absorbed energy [12]. Moreover the laser melting process can be considered as "high power density short interaction time" as reported by Kruth et al. [4], Simchi [7] Marangoni convection, also called surface-tension-driven convection or thermo-capillary convection, is well known phenomena in laser melting process. It can have a dramatic effect on the penetration depth of the resultant melt pool [15, 16].The Marangoni effect (also called the Gibbs–Marangoni effect) is the mass transfer along an interface between two fluids due to surface tension gradient. The temperature driven marangoni flow also referred as the thermo capillary convection is of primary importance in the selective laser melting [16]. Lei et al. [17] introduced mass, momentum and energy equations to model the fluid and temperature field in molten pool. In general when the temperature increases, the Marangoni forces decrease. However the Marangoni forces increase in the presence of surface active elements with increase in temperature [18].

During laser melting, localized powder melting occurs and a temperature gradient will be formed at the centre of the molten pool due to the Gaussian laser beam. Either concentration differences or temperature gradient at solid liquid interfaces within the pool may generate surface tension gradients and resultant Marangoni flow [19, 20].The total Marangoni flow, thus, can be divided into two parts: the thermal Marangoni flow and the solutal one [21, 22]. Based on Gu and Shen [23] experimental results, the thermal component of Marangoni flow will lead to a clockwise flow pattern (defined as source flow), whereas the solutal one does the opposite (defined as converging flow); the clockwise thermal component is weaker than the counterclockwise solutal one [24, 25] Marangoni effect plays a major role in SLM process, since this effect have not been studied in detailed for SS 316 L, this paper mainly discuss about the energy density, Marangoni flow and absorptivity happens during laser sintering process of SS316L powder.

## 2. Mathematical Model

### 2.1. Energy penetration

The main factors which affect the penetration of heat energy are the power of the laser beam, absorptivity of powder material, powder particle size distribution, powder density, and chemical constitution of the powder. Experimental studies of the reflection of the laser radiation by powder beds indicated that the absorptance of powder is considerably higher than the absorptance of the same material in the dense form [25, 26]. The theoretical analysis by the ray tracing computer simulation and the homogenized radiation transfer equation (RTE) revealed the universal function of the absorptance of the powder bed at normal incidence versus the absorptance of the same material in the dense form [27, 28]. Scheuren [29] pointed out that the laser radiation was not absorbed at the surface but penetrated into the powder bed.

It should noted that the freshly deposited powder is not mechanically compressed in many of the additive manufacturing processes to prevent damage to the previously processed underlying layer of the consolidated component. Therefore, the top powder layer has high porosity usually in the range 40–60% for typical metallic powders employed in additive processes [30, 31].

Laser radiation penetrates into powder through pores to a depth of several particle diameters because of multiple reflections as reported by Wang et al. [27]. This is comparable with the powder layer thickness. Thus, laser energy is deposited not on the surface but in the bulk of the powder layer. Yadroitsev et al. [11] reported the solutions to energy balance equations for the heat transfer through porous powder layer and it is given in Eqs. (2) to (5). In case of a powder surface, we implement of dimensionless number

$$D = (1-a)[1-a-\rho(1+a)]e^{-2a\lambda} - (1+a)[1+a-\rho(1-a)]e^{2a\lambda} \tag{2}$$

Absorptivity of the system powder-substrate is defined as the fraction of the incident radiation passing the powder surface, and is estimated as:

$$A_{ps} = \frac{\rho a}{(4\rho-3)D}\left\{2(1-\rho^2)e^{-\lambda} - (3+\rho e^{-2\lambda})\times\left\{\begin{matrix}[1+a-\rho(1-a)]e^{2a\lambda} + \\ [1-a-\rho(1+a)]e^{-2a\lambda}\end{matrix}\right\} - \frac{3(1-\rho)(1-\rho e^{-2\lambda})}{4\rho-3}\right. \tag{3}$$

The fraction of incident radiation absorbed by the substrate is

$$A_s = \frac{\rho a}{(4\rho-3)D}\left\{ (1-\rho^2)e^{-\lambda}[(1-a)e^{-2\lambda} + (1+a)e^{2a\lambda}] - 2(1-\rho)(3+\rho e^{-2\lambda}) \right\} - \frac{3(1-\rho)^2 e^{-\lambda}}{4\rho-3} \tag{4}$$

Absorptivity of the powder

$$A_p = A_{ps} - A_s \tag{5}$$

The hemispherical reflectivity of pure iron $\rho$ =0.7 is accepted for steel 316L. This is consistent with experimental data for powders of this stainless steel as indicated [26, 28]. Assuming that the powder bed consists of spherical particles of diameter D distributed in space, $\beta$ is the extinction coefficient, $\lambda$ is the optical depth and layer thickness is denoted by $L$.

$$\lambda = \beta L = \frac{3}{2}\frac{1-\varepsilon}{\varepsilon}\frac{L}{D} \tag{6}$$

## 2.2. Marangoni effect

According to Arafune and Hirata [22] the dimensionless Marangoni number ($M_a$) can be defined by:

$$\mathrm{Ma} = \frac{\Delta\sigma L}{\mu v} \tag{7}$$

where $\Delta\sigma$ is the surface tension difference of Marangoni flow (N/m), $L$ is the length of the free surface (m), $\mu$ is the dynamic viscosity (Pa ·s), and $v$ is the kinematic viscosity ($m^2$/s). Equation (7) reveals that $M_a$ is inversely proportional to $\mu$. For a low liquid content, the total intensity of Marangoni flow within the pool is limited, due to a higher $\mu$ of molten materials.

Numerical simulations are highly helpful in conducting these studies and visualizing the Marangoni flow. Navier-Stokes Eq. (8) which describes the

stationary momentum balance describes the velocity field and pressure distribution [32, 33].

$$-\eta\nabla^2 u + \rho u.\nabla u + \nabla p = F \tag{8}$$

$$\nabla u = 0$$

where $\eta$ is the dynamic viscosity (kg/(m·s)), $u$ is the velocity vector (m/s), $\rho$ is the density (kg/m$^3$) and $p$ is the pressure (Pa). The $F$ term is a source term representing external forces per unit volume (N/m$^3$).

The first term indicates the momentum transfer, viscous force, convective force and pressure force is indicated by the second and the third term respectively. The Marangoni effect which is induced at the interface is described by the following equation

$$\eta\frac{\partial u}{\partial y} = \gamma\frac{\partial t}{\partial x} \tag{9}$$

Here the shear stress on the surface is proportional to the temperature gradient. By solving the Navier-Stokes Eq. (8) the momentum transfer, pressure build up, viscous force and convective force can be found out. For simulating the nature of Marangoni flow 0.1× 0.1 mm dimension is selected from the continuous laser tracks.

## 2.3. Shrinkage

Shrinkage percentage has been calculated by using the following equation [34].

$$\text{Shrinkage } \% = \frac{L_c - L_m}{L_c} \times 100 \tag{10}$$

From the equation $L_c$ Original model dimension which is 100 μm and $L_m$ Measured dimension on the specimen which is after laser sintering of the powder particle.

## 3. Experimental Observation

In order to study the physical phenomena during laser sintering process, the stainless steel powder was spread over the pre heated stainless steel substrate (800°C) and the thickness of the powder layer is controlled to 100 μm using a scraper blade. Nd: YAG pulsed laser JK 300P (UK) was used for single track formation by varying the laser power, scanning speed and beam size. For conducting the experiments, Taguchi L9 orthogonal array has been followed as shown in Table 1.

One single laser track was made over the substrate and the SEM surface morphology has been shown in Fig. 3 for continuous track. The macrograph of laser tracks obtained for different process parameters are shown in Fig. 4. From the macrograph it is clearly visible that several continuous tracks were formed at different laser process parameters especially Figs. 4(d), (f), and (g). Moreover the laser parameter which produces continuous tracks which were mainly of higher laser energy density as referred in Table 1.

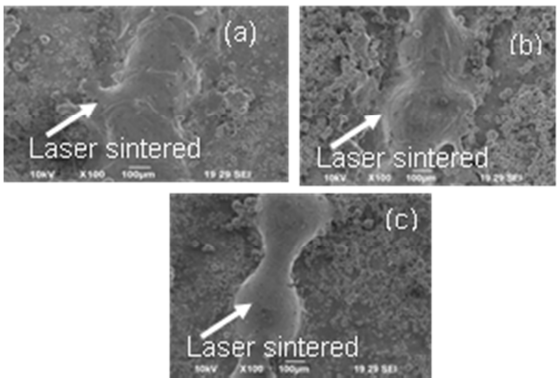


**Fig. 3. (a) Laser power: 150 W; laser speed: 2.4 m/min; beam size: 400 µm (b) Laser power: 150 W; laser speed: 12 m/min; beam size: 300 µm. (c) Laser power: 200 W; laser speed: 8.4 m/min; beam size: 300 µm.**

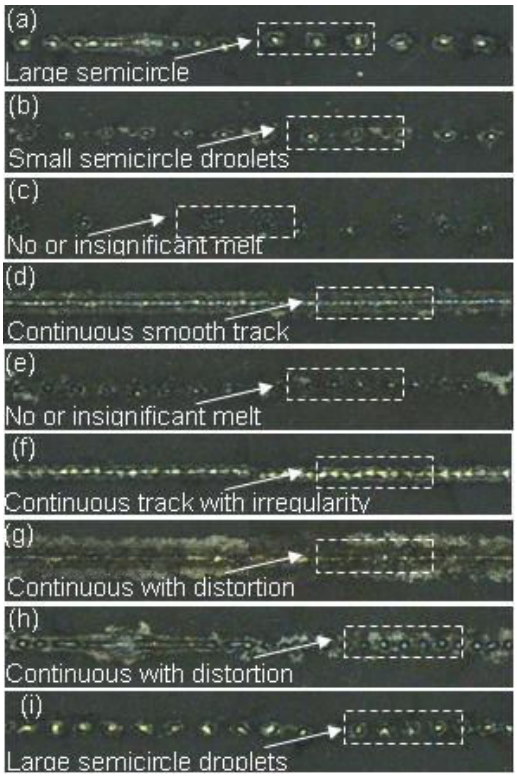


**Fig. 4. The macrograph of single track formation of SS 316L powder on SS 316L substrate (a) P 100 W; V 2.4 m/min; d 300 µm; (b) P 100 W; V 8.4 m/min; d 400 µm; (c) P 100 W; V 12 m/min; d 500 µm(d) P 150 W; V 2.4 m/min; d 400 µm; (e) P 150 W; V 8.4 m/min; d 500 µm; (f) P 150 W; V 12 m/min; d 300 µm(g) P 200 W; V 2.4 m/min; d 500 µm; (h) P 200 W; V 8.4 m/min; d 300 µm; (i) P 200 W; V 12 m/min; d 400 µm.**

**Table 1. The selected process parameters for laser melting for making single layer track using Taguchi L9 orthogonal array.**

| Trial No | Laser Power W | Laser Speed m/min | Beam Size µm | Energy Density J/mm$^2$ |
|---|---|---|---|---|
| **1** | 100 | 2.4 | 300 | 8.33 |
| **2** | 100 | 8.4 | 400 | 1.785 |
| **3** | 100 | 12 | 500 | 1 |
| **4** | 150 | 2.4 | 400 | 9.375 |
| **5** | 150 | 8.4 | 500 | 2.142 |
| **6** | 150 | 12 | 300 | 2.5 |
| **7** | 200 | 2.4 | 500 | 10 |
| **8** | 200 | 8.4 | 300 | 4.761 |
| **9** | 200 | 12 | 400 | 2.5 |

## 4. Results and Discussions

### 4.1. Shrinkage vs. energy density

The energy density versus shrinkage (Fig. 5) shows that at lower energy density the shrinkage is larger. This is mainly due to the laser power and the scan speed, which define the energy density which improperly melts the powder. The shrinkage decreases with increasing scan speed as well as the laser power (Fig. 5).

By increasing the energy density predominantly, the percentage of shrinkage will be reduced. Moreover by increasing the energy density up to certain limit (5 J/mm$^2$-8 J/mm$^2$), the material encounters higher degree of shrinkage. This is mainly due to the dissipation of higher laser energy into the powder bed and the molten pool becomes less viscous, thus, upon solidification. However, by increasing the energy density beyond this maximum, the strength of the part will be decreased because of a thermal damage. Moreover, the dependence on laser power is more pronounced, i.e., heat penetration mainly depends only on laser power which directly affects the percentage of shrinkage in the melted layer.

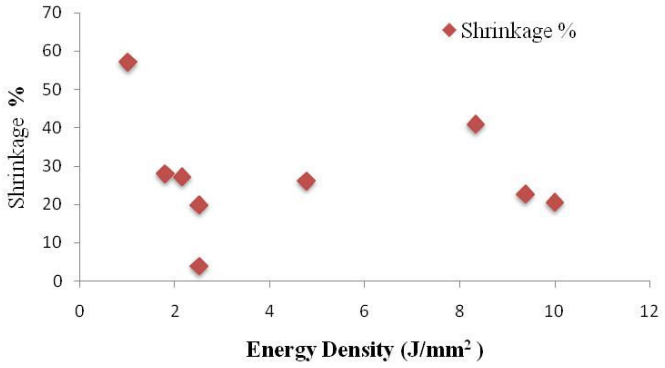


**Fig. 5. Shrinkage vs. Energy density.**

Therefore, it was found out that better densification rate of the powder was achieved at lower energy density the. It is to be noted that at high laser energy density, the intensity of the laser is large enough to cause the powder material to

vaporise. The laser melting can be considered as "high power density short interaction time" process. The delivered energy heats up the exposed powder particles rapidly beyond the melting temperature. The particle bonding is then performed and the kinetics of densification depends on the working temperature. Consequently, the parameters involved in determining the method of energy delivered to the powder medium control the melting rate. Meanwhile, the evaporation of exposed powder in the laser melting process may occur, particularly at an intensive laser energy input. It was found that as the laser energy input increases better densification is achieved. Nevertheless, there is a saturation level, beyond which, full density cannot be obtained even at very intensive laser energy.

## 4.2. Absorptivity

Figures 6 to10 represent the porosity ranging from 40-60%. It has been reported that the porosity of metallic powders used for laser melting processes are in the range of 40-60% [10]. At different percentage of porosity, the total Absorptivity of powder as well as substrate has been found out and the same represented in Figures 6 to 10. From the mathematical model, it is noticed that the low optical depth leads to higher absorptivity of powder, whereas it is decreasing when exposed in higher optical depth for all the percentage levels. At higher optical depth scattering of laser light doesn't happen so the light escapes without scattering, scattering of laser light in the powder bed mainly leads to absorption. When comparing the percentage of porosity, at higher porosity the numerical model shows a higher absorption in powder as well as the substrate, when porosity is higher the voids spaces in the powder bed is higher so the powder particles will absorb more laser energy. Other graphs showing more or less same deflection range.

Furthermore, in all the range of porosity (40-60%) the maximum absorptivity of powder is less than 0.9 as shown in Figs. 6 to 10. Absorptivity of the powder-substrate (Aps) is calculated from Eq. (3). The fraction of incident laser radiation absorbed by the substrate calculated from Eq.(4) and absorptivity of the powder is represented as (Ap) Eq.(5).

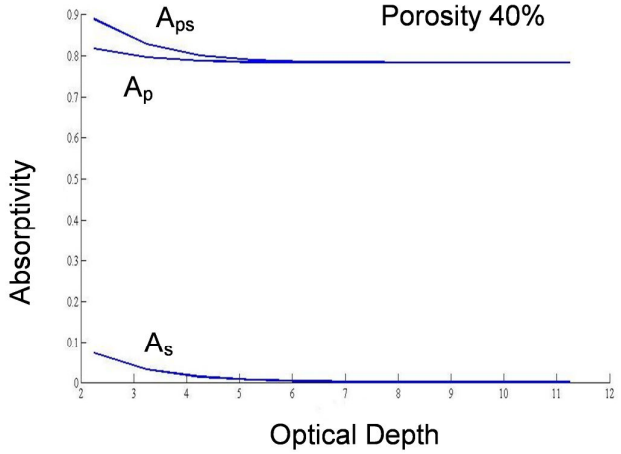


**Fig. 6. Total absorptivity versus optical depth at porosity 40%.**

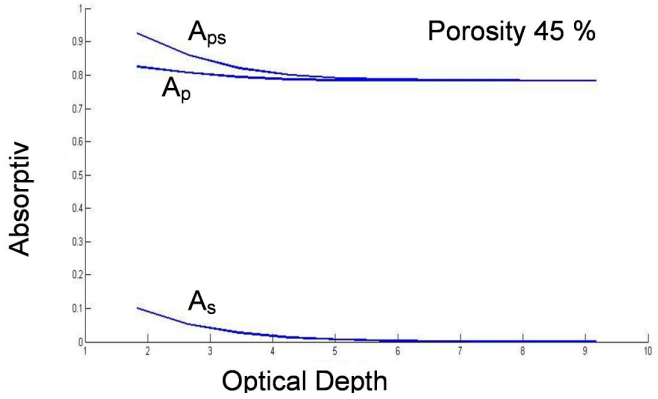


**Fig. 7. Total absorptivity versus optical depth at porosity 45%.**

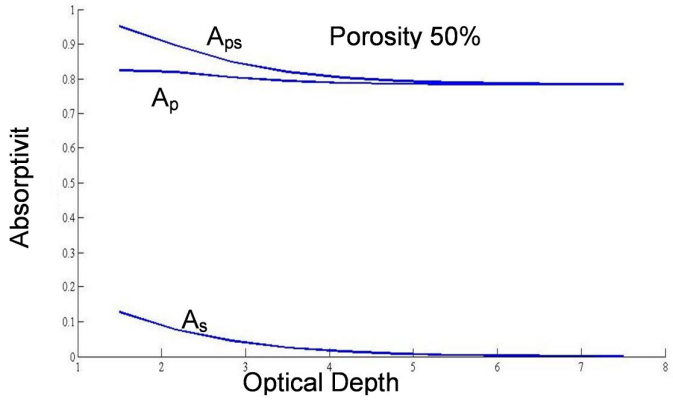


**Fig. 8. Total absorptivity versus optical depth at porosity 50%.**

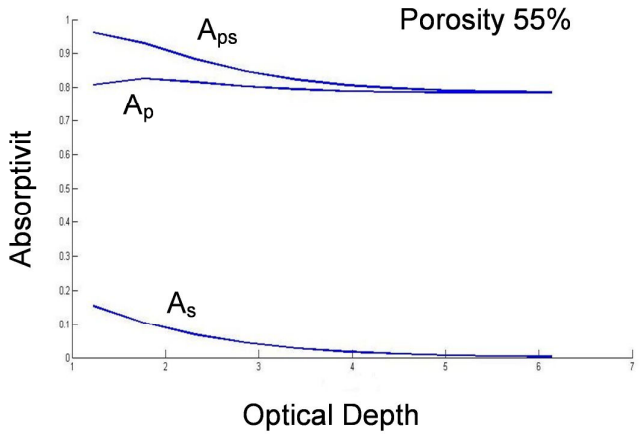


**Fig. 9. Total absorptivity versus optical depth at 55%.**

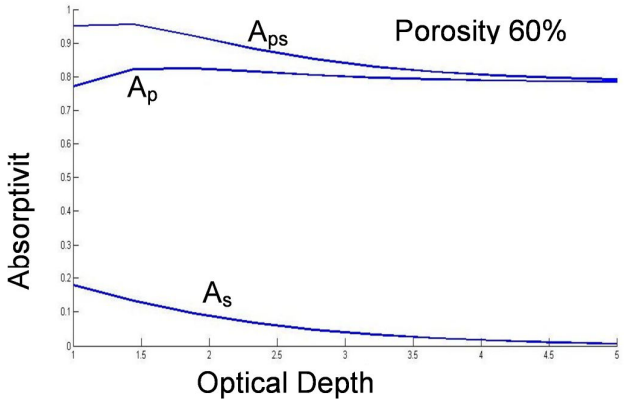


**Fig. 10. Total absorptivity versus optical depth at porosity 60%.**

### 4.3. Marangoni Flow

The simulation of Marangoni flow is carried out using the parameters listed in Table 2. Laser energy density which produces continuous track has been selected for Marangoni flow studies. Figures 11 to 13 show the Marangoni flow at different laser power. Two types of Marangoni flow identified during simulation are source flow and solutal one.

At laser energy density 2.5 J/mm$^2$, 4.761 J/mm$^2$ and 9.375 J/mm$^2$ from Figs. 11 to 13 indicates flow pattern leads to a clockwise direction which is known as source flow, whereas at high laser density the flow pattern direction is counter clockwise which is solutal one. The clockwise thermal component (source flow) is weaker than the counterclockwise solutal one. Meanwhile, the comparatively stronger solutal counter clockwise Marangoni flow continuously drives the particles in the melt pool, gathering the particles around the center resulting in a wider and deeper melt pool at higher energy density.

At higher energy density the melt pool is comparatively bigger so the convection effect will be higher depicts in Fig. 13. Thus Marangoni flow plays a major role in producing continuous smooth track for the higher energy density of 9.375 J/mm$^2$ Fig. 4(d). As the value of surface tension is negative the higher surface tension of the cooler liquid pool tends to pull the liquid metal away from the centre of the liquid pool, where the liquid metal is hotter and surface tension is lower. Fluid flow on the surface is radically outward, It is also clear that the Marangoni flow influences the flow of the fluid in the specimen and the distribution of temperature. The convection direction can be seen which is represented by the arrows taking place in the clockwise direction (Figs. 11 to 13) the convection here is essentially a free convection. The magnitude of the molten fluid flow mainly depends on the viscosity, surface tension gradient, temperature gradient and thermal diffusion. But when the liquid pool gets larger than the beam diameter due to higher laser power, Marangoni eddies appear at the periphery of the laser pool owing to the large surface thermal gradients. This convection largely affects the traces by widening them and/or deepening them at their centre.

**Table 2. Parameters for simulation of Marangoni effect.**

| Parameters | Value |
|---|---|
| **Laser Energy Density (J/mm$^2$)** | 2.5, 4.761, 9.375 |
| **Density (kg/m$^3$)** | 7200 |
| **Viscosity (kg/m-s)** | 0.05 |
| **Thermal conductivity (W/m-K)** | 16.2 |
| **Heat capacity (J/kg-K)** | 502 |
| **Thermal expansion co-efficient (1/K)** | $17.3\times10^{-6}$ |

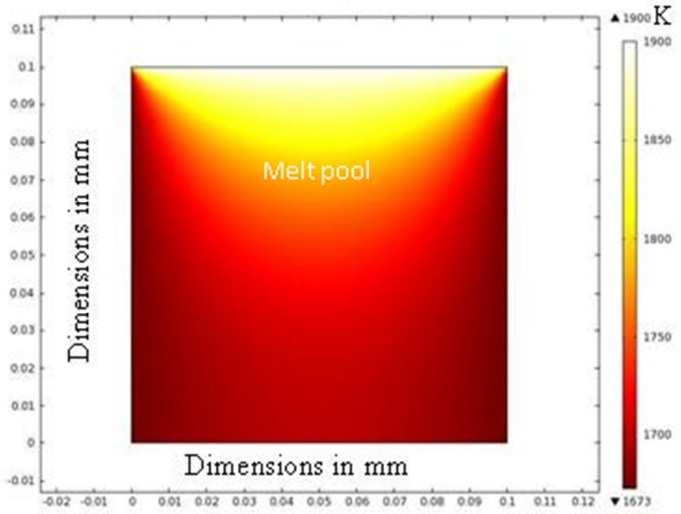


**Fig. 11(a). Temperature distribution at laser energy density 2.5 (J/mm$^2$).**

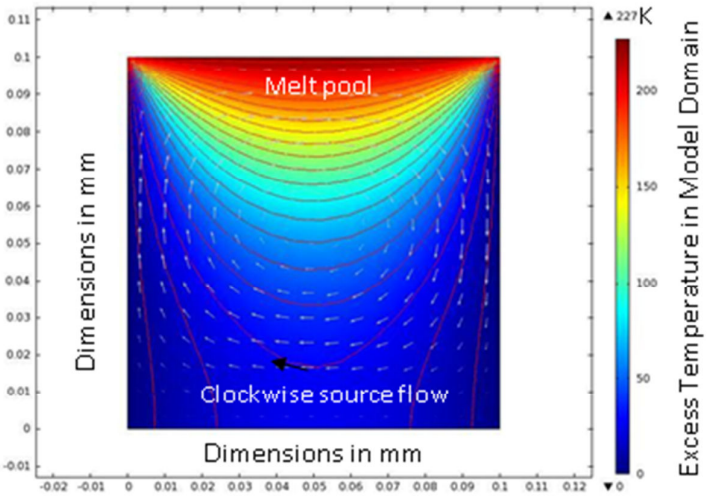


**Fig. 11(b). Marangoni effect at laser energy density 2.5 (J/ mm$^2$).**

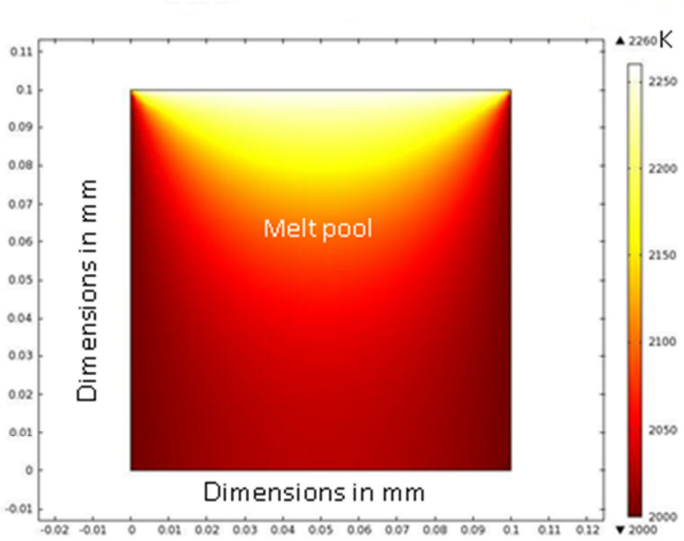


**Fig. 12(a). Temperature distribution at laser energy density 4.761 (J/ mm$^2$).**

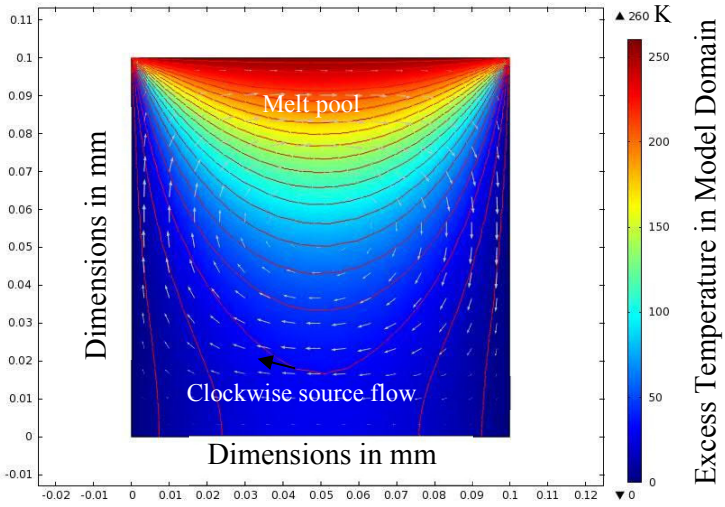


**Fig. 12(b). Marangoni effect at laser energy density 4.761(J/ mm$^2$).**

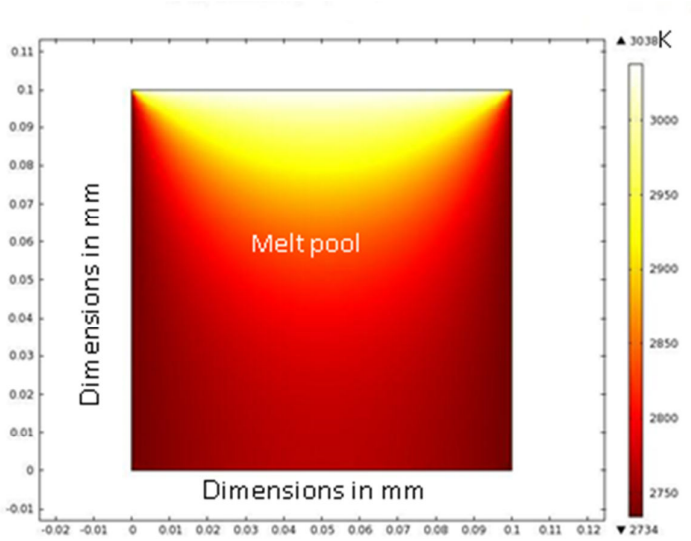


**Fig. 13(a). Temperature distribution at laser energy density 9.375 (J/ mm$^2$).**

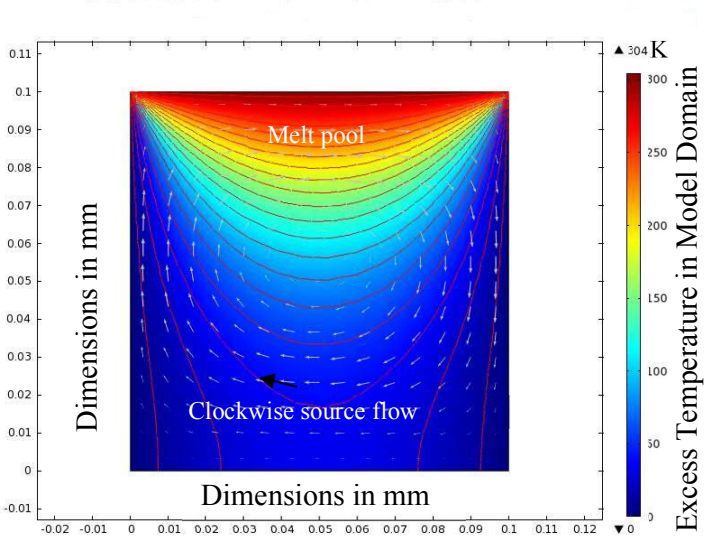


**Fig. 13(b). Marangoni effect at laser energy density 9.375 (J/ mm$^2$).**

## 5. Conclusion

Different factors like energy density, shrinkage, absorptivity and Marangoni flow were studied for laser melted SS316L powder. The numerical results indicate a clear cut idea on how the energy density influences the shrinkage as well as Marangoni flow. The absorptivity of the powder plays a crucial role in

consolidation phenomena of the powder layer which helps to get a denser part or layer. Due to Marangoni flow there is significant amount of heat distribution throughout the powder bed. The influence of Marangoni convection can lead to form a crater or can be described as a distinct surface roughness which is kind of a signature of the laser processing conditions. At energy density 9.375 J/mm$^2$ the Marangoni effect is minimum and the experimental result (Fig. 4(d)) validates the multi physics model by giving a smooth and continuous track. Laser Power as well as scanning speed has to be refined so as to make the process perfect. The physical phenomena such as evaporation and radiation are neglected during the modelling hence in the upcoming works all the factors has to be considered to get a real time study results for laser melting process.

## References

1. Williams, J.D.; and Deckard, C.R. (1998). Advances in modeling the effects of selected parameters on the SLS process. *Rapid Prototyping Journal*, 4(2), 90-100.
2. Shishkovsky, I.; Morozov, Yu.; and Smurov, I. (2007). Nanofractal surface structure under laser sintering of titanium and nitinol for bone tissue engineering. *Applied Surface Science*, 254(4), 1145-1149.
3. Yadroitsev, I.; Bertrand, P.H.; and Smurov, I. (2007). Modelling of radiation and heat transfer at selective laser melting. *Applied Surface Science*, 253, 8064.
4. Kruth, J.P.; Froyen, L.; Vaerenbergh, J.V.; Mercelis, P.; Rombouts, M.; and Lauwers, B. (2004). Selective laser melting of iron-based powder. *Journal of Materials Processing Technology*, 149(1-3), 616-622.
5. Das, S. (2003). Physical aspects of process control in selective laser sintering of metals. *Advanced Engineering Materials*, 5(10), 701-711.
6. Osakada, K.; and Shiomi, M. (2006). Flexible manufacturing of metallic products by selective laser melting of powder. *International Journal of Machine Tools and Manufacture*, 46(11), 1188-1193.
7. Simchi, A. (2006). Direct laser sintering of metal powders: Mechanism, kinetics, and microstructural features. *Material Science and Engineering A*, 428(1-2), 148-158.
8. Xu, L.K.; Shen, Y.; and Gu, D. (2004). Progress in temperature field research into selective laser sintering process. *Foundry*, 7(53), 511-514.
9. Bai, P.-K.; Cheng, J.; Liu, B.; and Wang, W.-F. (2006). Numerical simulation of temperature field during selective laser sintering of polymer-coated molybdenum powder. *Transaction of Nonferrous Metal Society of China*, 16(2), 603-607.
10. Gusarov, A.V.; Yadroitsev, I.; Bertrand, Ph.; and Smurov, I. (2009). Model of radiation and heat transfer in laser-powder interaction zone at selective laser melting. *Journal of Heat Transfer ASME*, 131(7), 072101-10.
11. Yadroitsev, I.; Gusarov, A.; Yadroitsava, I.; and Smurov, I. (2010). Single track formation in selective laser melting of metal powders. *Journal of Materials Processing Technology*, 210(12), 1624-1631.

12. Alessandro, F.; Michele, L.; and Luca, R. (2010). Experimental analysis of selective laser sintering of polyamide powders an energy perspective. *Journal of Cleaner Production*, 18(16-17), 1722-1730.
13. Kizaki, Y.; Azuma, H.; Yamazaki, S.; Sugimoto, H.; and Takagi, S. (1993). Phenomenological studies in laser cladding. Part I. Time-resolved measurements of the absorptivity of metal powder. *Japan Journal of Applied Physics,* 32(1), 205-212.
14. Fischer, P.; Leber, H.; Romano, V.; Weber, H.P.; Karapatis, N.P.; André, C.; and Glardon, R. (2004). Microstructure of near infrared pulsed laser sintered titanium samples. *Applied Physics A*, 78(8), 1219 -1227.
15. Limmaneevichitr, C.; and Kou, S. (2000). Visualization of Marangoni convection in simulated weld pools. *Welding Research Supplement*. 126-135.
16. Bin X.; and Yuwen, Z. (2008). Numerical simulation of direct metal laser sintering of single-component powder on top of sintered layers. *Journal of Manufacturing Science and Engineering*, 130(4), 041002-10.
17. Lei, Y.P.; Murakawa, H., Shi, Y.W.; and Li, X.Y. (2001). Numerical analysis of the competitive influence of Marangoni flow and evaporation on heat surface temperature and molten pool shape in laser surface remelting. *Computational Materials Science*, 21(3), 276-290.
18. Shoo, P.; Collur, M.M.; and Debroy, T. (1988). Effect of oxygen and sulphur on alloying element vaporization rates during laser welding. *Journal of Material Transaction B*, 19(6), 967-972.
19. Niu, H.J.; and Chang, T.H.; (1999). Instability of scan tracks of selective laser sintering of high speed steel powder. *Scripta Materilia*, 41(11), 1229-1234.
20. Gu, D.D.; Shen, Y.F.; Zhao, L.; Xiao, J.; Wu, P.; and Zhu, Y.B. (2007). Effect of rare earth oxide addition on microstructures of ultra-fine WC-Co particulate reinforced Cu matrix composites prepared by direct laser sintering. *Material Science and Engineering A*, 445-446, 316-332.
21. Yin, H.B.; and Emi, T. (2003). Marangoni flow at the gas/melt interface of steel. *Metallurgical and Material Transaction B,* 34(5), 483-493.
22. Arafune, K.; and Hirata, A. (1999). Thermal and solutal Marangoni convection in In–Ga–Sb system. *Journal of Crystal Growth*, 197(4), 811-817.
23. Gu, D.; and Shen, Y. (2008). Influence of Cu-liquid content on densification and microstructure of direct laser sintered submicron W–Cu/micron Cu powder mixture. *Materials Science and Engineering A*, 489(1-2), 169-177.
24. Rohit, T; Kurian, A.; Senthilkumaran, K.; and Arivazhagan, N. (2013). Studies on absorptivity and Marangoni flow during laser sintering. *Advanced Materials Research*, 622- 623, 531-534.
25. Tolochko, N.K.; Laoui, T.; Khlopkov, Y.V.; Mozzharov, S.E.; Titov, V.I.; and Ignatiev, M.B. (2000). Absorptance of powder materials suitable for laser sintering. *Rapid Prototyping Journal*, 6(1), 155-160.
26. Gusarov, A.V.; Bentefour, E.H.; Rombouts, M.; Froyen, L.; Glorieux, C.; and Kruth, J.P. (2006). Normal directional and normal-hemispherical reflectances of micron- and submicron-sized powder beds at 633 and 790 nm. *Journal of Applied Physics*, 99, 113528.

27. Wang, X.C.; Laoui, T.; Bonse, J.; Kruth, J.P.; Lauwers, B.; and Froyen, L. (2002). Direct selective laser sintering of hard metal powders: experimental study and simulation. *International Journal of Advanced Manufacturing Technology,* 19(5), 351-357.
28. Gusarov, A.V.; and Kruth, J.P. (2005). Modelling of radiation transfer in metallic powders at laser treatment. *International Journal of Heat and Mass Transfer*, 48(16), 3423-3434.
29. Scheuren, B.V.; (1996). *Basic contribution to the development of the selective metal powder sintering process*. Ph.D. thesis, K.U. Leuven, Belgium.
30. Florencia, E.W.; Kah F.L.; and Chee, K.C. (2010). Modeling of powder particle heat transfer process in selective laser sintering for fabricating tissue engineering scaffolds. *Rapid Prototyping Journal*, 16(6), 400-410.
31. Rombouts, M.; Kruth, J.P.; Froyen, L.; and Mercelis, P. (2006). Fundamentals of selective laser melting of alloyed steel powders. *CIRP Annals-Manufacturing Technology*, 55(1), 187-192.
32. Levich, V.G. (1962). *Physicochemical hydrodynamics*. Prentice-Hall, N.J.
33. Jean, M.D.; Sébastien, P.; Cyrille, B.; and Sélim, M. (2004). Modelling Marangoni convection in laser heat treatment. *Journal de Physique IV*, 120, 299-306.
34. Ning, Y.; Wong, Y.S.; and Fuh, J.Y.H. (2005). Effect of control of hatch length on material properties in the direct laser sintering process. *Journal of Engineering Manufacture*, 219(1), 15-25.